Cerebral Cortex, October 2017;27: 4835–4850

doi: 10.1093/cercor/bhw280
Advance Access Publication Date: 12 September 2016
Original Article

ORIGINAL ARTICLE

Layer-Specific Refinement of Sensory Coding in Developing Mouse Barrel Cortex

Alexander van der Bourg[1,2,5], Jenq-Wei Yang[3,5], Vicente Reyes-Puerta[3], Balazs Laurenczy[1,2], Martin Wieckhorst[1], Maik C. Stüttgen[4], Heiko J. Luhmann[3,6], and Fritjof Helmchen[1,2,6]

[1]Laboratory of Neural Circuit Dynamics, Brain Research Institute, University of Zurich, CH-8057 Zurich, Switzerland, [2]Neuroscience Center Zurich, University of Zurich and ETH Zurich, CH-8057 Zurich, Switzerland, [3]Institute of Physiology, University Medical Center of the Johannes Gutenberg University, D-55128 Mainz, Germany, [4]Institute of Pathophysiology, University Medical Center of the Johannes Gutenberg University, D-55128 Mainz, Germany, [5]Co-first authors, and [6]Co-senior authors

Address correspondence to Fritjof Helmchen (Email: helmchen@hifo.uzh.ch) and Heiko J. Luhmann (Email: luhmann@uni-mainz.de)

Abstract

Rodent rhythmic whisking behavior matures during a critical period around 2 weeks after birth. The functional adaptations of neocortical circuitry during this developmental period remain poorly understood. Here, we characterized stimulus-evoked neuronal activity across all layers of mouse barrel cortex before, during, and after the onset of whisking behavior. Employing multi-electrode recordings and 2-photon calcium imaging in anesthetized mice, we tested responses to rostro-caudal whisker deflections, axial "tapping" stimuli, and their combination from postnatal day 10 (P10) to P28. Within this period, whisker-evoked activity of neurons displayed a general decrease in layer 2/3 (L2/3) and L4, but increased in L5 and L6. Distinct alterations in neuronal response adaptation during the 2-s period of stimulation at ~5 Hz accompanied these changes. Moreover, single-unit analysis revealed that response selectivity in favor of either lateral deflection or axial tapping emerges in deeper layers within the critical period around P14. For superficial layers we confirmed this finding using calcium imaging of L2/3 neurons, which also exhibited emergence of response selectivity as well as progressive sparsification and decorrelation of evoked responses around P14. Our results demonstrate layer-specific development of sensory responsiveness and response selectivity in mouse somatosensory cortex coinciding with the onset of exploratory behavior.

Key words: barrel cortex, calcium imaging, development, response selectivity

Introduction

Neurons in the "barrel" subfield of rodent primary somatosensory cortex (S1) encode information about whisker movement and touch. Neurons in layer 4 (L4) of barrel cortex form cellular aggregates (the "barrels"), which define cortical columns that are topographically related to individual whiskers on the contralateral side of the snout (Woolsey and van der Loos 1970). Although the formation and anatomical refinement of barrel cortex organization during development has been extensively studied (van der Loos and Woolsey 1973; Erzurumlu and Gaspar 2012; Feldmeyer et al. 2013), little is known about the corresponding functional changes, especially how whisker-evoked cortical activity develops at the onset of active whisking behavior.

In rodents, active whisking behavior matures during the first 3 postnatal weeks. More specifically, vibrissa movements

transition from spontaneous unilateral muscle twitches of the whisker pad, as they occur in the first week, to regular and bilateral rhythmic whisking at the end of the third postnatal week (Grant et al. 2012; Arakawa and Erzurumlu 2015). At around P13, cortical connectivity and excitability undergo major re-organization. Potentiation of excitatory synapses between L4 and L2/3 is followed by strengthening of local connectivity between neurons in L2/3 (Clem and Barth 2006; Clem et al. 2008; Wen and Barth 2011; Itami and Kimura 2012). In rat barrel cortex, whisker-evoked synaptic potentials are detectable around P12 in L4, but only at P14 in L2/3 suggesting a critical period for L4 to L2/3 connectivity (Stern et al. 2001). In parallel to these changes in synaptic drive, intrinsic excitability of pyramidal neurons in superficial L2/3 markedly decreases (Maravall et al. 2004; Borgdorff et al. 2007), while synapse density (Micheva and Beaulieu 1996; Chandrasekaran et al. 2015) and spine turnover (Lendvai et al. 2000) increases in the second postnatal week. These changes in intrinsic excitability and synaptic connectivity are also reflected by a switch of spontaneous activity from highly correlated bursts of action potential firing (Khazipov and Luhmann 2006; Yang et al. 2009) to desynchronized and sparse activity (Golshani et al. 2009). Similar results have been described for postnatal development of other sensory cortices like mouse visual cortex (Rochefort et al. 2009). In addition, direction selectivity in visual cortex was found to be present before eye opening, not requiring visual experience (Rochefort et al. 2009, 2011; Hagihara et al. 2015). However, it is largely unknown how processing of tactile stimuli with different directional forces, an important function for texture discrimination, develops across the neocortical layers in the maturing barrel cortex during this critical period.

Whisker forces and kinematics convey important information for rodent perception (Gopal and Hartmann 2007; Chen et al. 2013). Most studies on barrel cortex have used controlled lateral deflections of single or multiple whiskers. Such lateral deflections for example occur when animals have to discriminate the width of an aperture (Krupa et al. 2001). The development of direction selectivity to lateral whisker deflections with varying stimulation angles has been reported to develop in the fourth postnatal week in rat barrel cortex (Kremer et al. 2011). However, a behaviorally relevant whisker force component is touch-induced whisker bending, which exerts an axial force on the whisker follicle. Such axial whisker movements evoke strong responses in the trigeminal ganglion (Stüttgen et al. 2008) and are important for object localization (Pammer et al. 2013). How neurons in developing barrel cortex respond to axial or lateral whisker forces and how these response profiles relate to the development of exploratory whisking behavior have so far remain unexplored. We therefore aimed to investigate the maturation of sensory responses to distinct mechanical forces on the whisker follicle (laterally and axially, as they occur during brushing and tapping of objects, respectively; Quist et al., 2014) before, during, and after the onset of active whisking.

Using a novel whisker stimulator for both lateral and axial stimulation, we here examined how responses to these distinct stimuli of barrel cortex neurons change during the critical phase of postnatal development. We find that sensory-evoked activity matures in a layer-specific manner in a narrow time window around P13, at the onset of active locomotion and whisking. Stimulus-evoked activity in supragranular and granular layers generally decreases at this developmental stage whereas neurons in infragranular layers show increased responsiveness. We also demonstrate that during the same period neurons develop a higher selectivity for lateral or axial whisker forces, especially in L2/3. Together, these findings reveal substantial refinements of whisker-evoked activity in barrel cortex coinciding with the onset of explorative whisking behavior.

Materials and Methods

Animal experiments were approved by the Cantonal Veterinary Office Zurich and the local German ethics committee (#23177-07/G10-1-010), respectively. Experiments followed the European, German (European Communities Council Directive, 86/ 609/ECC), and Swiss national regulations.

Behavior Monitoring

Five C57BL/6 mice (3 males and 2 females of the same litter) were placed 2 times per day (2 min sessions) in a 75 × 60 cm^2 enclosed arena to assess locomotion and whisking behavior in darkness between P10 and P28 (Fig. 1 and Supplementary Movie 1). Movement trajectories were recorded at 15 frames per second (fps) at 1280 × 1024 pixels (LUMENERA Lw 570, Lumenera Coorp., ON, USA). The light-proof arena was illuminated by an infrared light emitting diode (LED) light source (730 nm, M730L4, Thorlabs Inc., USA). We traced movement trajectories semi-automatically with custom-written routines in MATLAB. Movement was scored as "whisking along walls" if (1) the mouse moved in close proximity to the arena wall while the whiskers touched the wall (head center distance to wall ≤3 cm) and (2) the animal was not at rest during wall touches. Whisking behavior was monitored for 5 min and assessed by a scoring scheme for active whisking (Landers and Philip Zeigler 2006).

Animal Surgery and Preparation

We used 18 C57BL/6 mice (9 males and 9 females) at ages ranging from P10 to P28 for multi-electrode recordings, and 18 C57BL/6 mice (10 males and 8 females) for 2-photon calcium imaging. Mice were sedated with chlorprothixene (0.1 g/kg, intraperitoneal (i.p.); Sigma-Aldrich Chemie GmbH, Buchs, Switzerland) and lightly anesthetized with urethane (0.25–0.5 g/kg, i.p.). Atropine (0.3 mg/kg; Sigma-Aldrich Chemie GmbH, Buchs, Switzerland) and dexamethasone (2 mg/kg; aniMedica GmbH, Senden-Bösensell, Germany) were administered subcutaneously (s.c.) to reduce secretion of saliva and to prevent edema (s.c. injection 30 min after induction of anesthesia). The body temperature was maintained at 37 °C with a heating blanket. Hydration levels were checked regularly and maintained by s.c. injections of Ringer-lactate (Fresenius Freeflex; Fresenius Kabi AG, Oberdorf, Switzerland). The depth of anesthesia was evaluated throughout the experiment by testing the pinch reflex on the forepaw. A custom-built head plate was glued to the skull over the left brain hemisphere with dental cement (Paladur, Heraeus Kulzer GmbH Hanau, Germany; Caulk Grip Cement for electrophysiology) to secure and stabilize the animal.

A small cranial window of 1.5 × 1.5 mm^2 was opened above the center of the mapped barrel columns with a sharp razor blade and superfused with Ringer's solution (in mM: 145 NaCl, 5.4 KCl, 10 HEPES, 1 $MgCl_2$, 1.8 $CaCl_2$; pH 7.2 adjusted with NaOH). Care was taken not to damage the dura or surface blood vessels in young animals (P10–P20). In animals older than P20, we removed the dura to prevent blockage of the glass pipette tip during insertion into the cortex for 2-photon guided calcium indicator loading. For multi-electrode recordings, the dura was

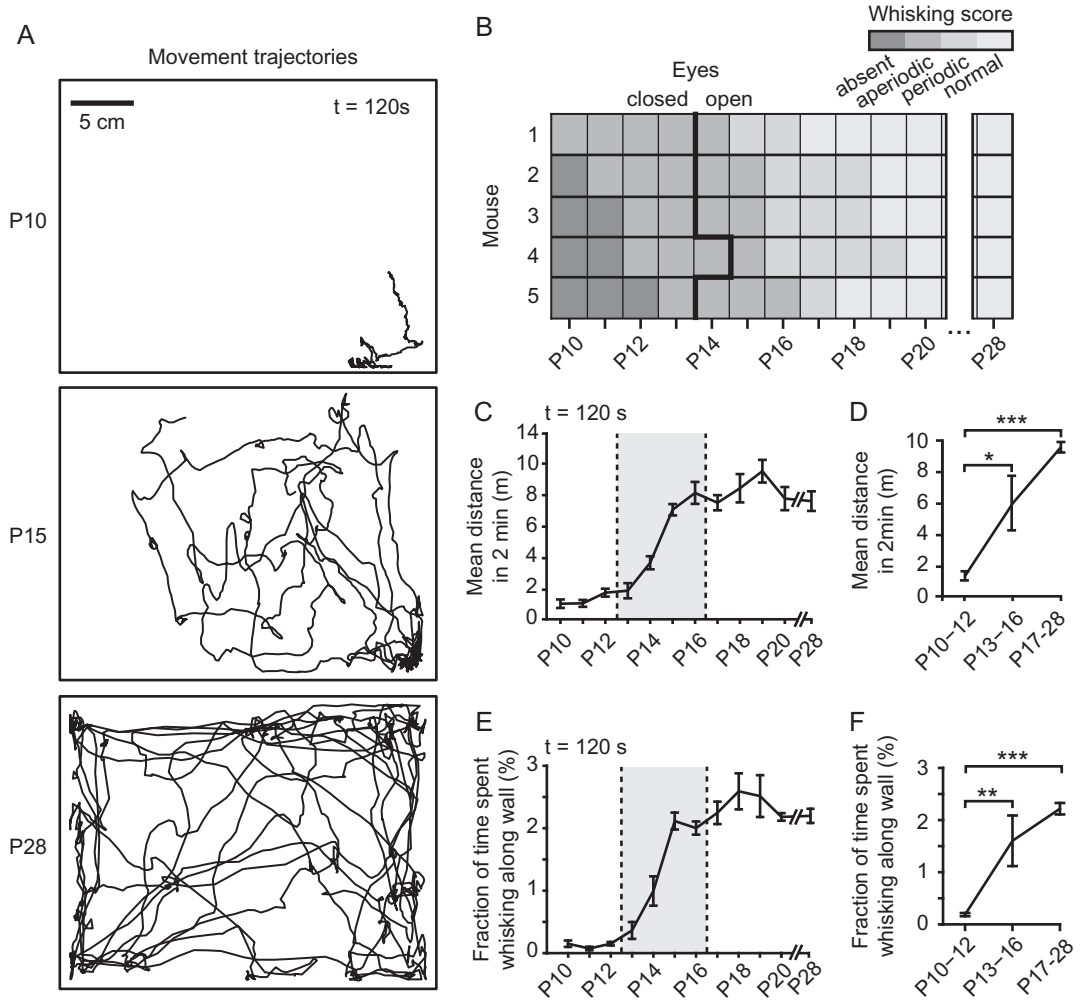

Figure 1. Postnatal development of explorative behavior in mice. (*A*) Movement trajectories in an open field arena, measured over 2 min for one example mouse at age P10, P15, and P28. (*B*) Quantification of whisking behavior of a litter of 5 mice from P10 to P28. Whisking was classified as absent (no whisking), aperiodic (small, aperiodic whisker movements), periodic (low amplitude whisking at 2–5 Hz), and normal (larger amplitude whisking at 5–15 Hz). Whisking classes are depicted as different grey levels. Time of eye opening is indicated by the thick line. (*C*) Quantification of the mean distance traveled during a 2-min observation time across days. Largest changes occurred in the P13–16 age group (grey box). (*D*) Pooled analysis of the mean distance traveled for the 3 age groups defined in C ($P = 0.02$ for P10–12 vs. P13–16; $P = 0.001$ for P10–12 vs. P17–28). (*E*) Quantification of time spent whisking along the walls of the arena during a 2-min observation time across days. (*F*) Pooled analysis of the fraction of time spent whisking along walls for the 3 age groups ($P = 0.0085$ for P10–12 vs. P13–16; $P = 0.0003$ for P10–12 vs. P17–28). Data points are mean ± s.e.m. ($n = 5$ mice). Statistics: Kruskal–Wallis test followed by Dunn–Sidak's post hoc correction (*$P < 0.05$, **$P < 0.01$, ***$P < 0.001$).

penetrated and the cranial window sealed with agarose (Type III-A, 1% in Ringer; Sigma).

Intrinsic Optical Imaging

The principal whisker-related barrel column was identified using optical imaging of intrinsic signals. The cortical surface was visualized through the intact bone by surface application of normal Ringer's solution and a glass coverslip placed on top. The skull surface above the barrel cortex was left intact for animals younger than P20, but thinned in older animals. Reference images of the cortical blood vessel pattern were visualized by a 546-nm LED to enhance contrast. Functional maps of the target barrel columns C1 and C2 were obtained by shining red light (630 nm LED) on the cortical surface while stimulating the C1 or C2 whisker with a piezoelectric element (10 Hz at 2° amplitude in rostrocaudal direction). Reflectance images were collected through a 4× objective with a CCD camera (Toshiba TELI CS3960DCL; 12-bit; 3-pixel binning, 427 × 347 binned pixels, 8.6 μm pixel size, 10 fps). Functional intrinsic signal images were computed as fractional reflectance changes relative to the pre-stimulus average (average of 30 trials). The intrinsic signal images obtained for the C1 or C2 barrel columns were then mapped to the blood vessel reference image and used to guide the location of the craniotomy.

Histology

After each experiment, the animal was deeply anesthetized with ketamine (120 mg/kg, ketamine, 50 mg/mL, Hameln Pharma, Hameln Germany) and xylazine (5 mg/kg, Rompun 2%, Bayer, Leverkusen, Germany) and perfused through the aorta with 0.2 M phosphate-buffered saline (PBS) for washing. The brain was carefully removed from the skull and kept in 4% paraformaldehyde for 24 h at 4 °C. After 24 h, the brain was washed with 0.1 M PBS and stored in 30% sucrose (in PBS) overnight. After washing with PBS, brains were sectioned in 200-μm thick tangential sections and prepared for cytochrome-oxidase (COX)

immunohistochemistry. Sections were rinsed in PBS and incubated at 39 °C in a solution of 0.6 mg cytochrome c, 0.5 mg DAB, and 44 mg sucrose per ml, with 0.3% catalase included. Sufficient staining of barrels was achieved after 2–7 h of reaction. After COX immunohistochemistry, sections were intensified with 0.5% copper(II) sulfate (Sigma) for 2–3 min, air dried, and mounted. All chemicals were obtained from Sigma (Deissenhofen, Germany).

Galvanometer-Driven Whisker Stimulation

We applied whisker stimulation with a novel galvanometer-driven stimulation system, consisting of 2 thin (200-μm diameter) optical fibers attached to the whisker, one for each stimulation axis (Fig. 2 and Supplementary Movie 2). Both fibers were glued together near their tips with 3 M Scotch Weld repositionable glue and the whisker was attached in its resting position to one optical fiber tip with a droplet of glue. Stimulation fibers were visually guided towards the whisker's resting position under a stereoscope with a micromanipulator. We kept the attachment position relative to the snout constant for all experiments (1 cm from follicle for both axial and lateral stimulation fiber). For each fiber, translation was controlled by a galvanometer (SpaceLas ILDA30kpps galvanometric system kit, Topic Light Co., Ltd, Guangdong, China). The rotational movement of the galvanometer was transformed into a translational movement by attaching the backend of the optical fiber to a small pole arm fixed on the galvanometer axis. Each optical fiber was embedded in a low friction heat resistant capillary tube (Polymicro, inner diameter: 251 μm, outer diameter: 355 μm; Molex, USA). A mounting point for each axis close to the stimulation site suppressed movement and vibrations of the outer fibers.

We used this 2-axis stimulator to mechanically deflect a single whisker in the rostrocaudal and mediolateral direction, respectively, thereby inducing whisker forces laterally and/or axially to the follicle base. Axial and lateral whisker movements were induced simultaneously or independently at high temporal and spatial resolution. The stimulation pulse consisted of a phase-shifted 100 Hz cosine, which was presented at a repetition rate of 4.76 Hz for 2 s (pulse amplitude: 1 mm; pulse duration 10 ms, inter-stimulus interval: 200 ms, resulting in 1140°/s maximum speed). Galvanometers were driven by generating analog output signals (5000 samples per second) through a NI PCIE-6323 card and controlled by custom-written LabVIEW software. During the experiment, we monitored consistent stimulation output from live feedback of the galvanometer positioning. Each stimulus type was presented 20 times, as random sequence of blocks of 5 stimuli, with each stimulus separated by an 8-s blank time (no stimulation). Stimulator performance was evaluated by imaging fiber-tip movements at high speed (5000 fps, Basler A504k, Basler Vision Technologies, Ahrensburg, Germany) and analyzing the fiber-tip trajectory horizontally and vertically. Custom-written software was used to semi-automatically measure the translational movement of each fiber for a given trial. Deviation of the translational movement from the template stimulus for each measured data point was below 100 μm. Movement trajectories of the C2 whisker were tracked with the Whisk tracking software (Clack et al. 2012) from high-speed image sequences (3000 fps). The extracted whisker envelope was low-pass filtered (5-point sliding average).

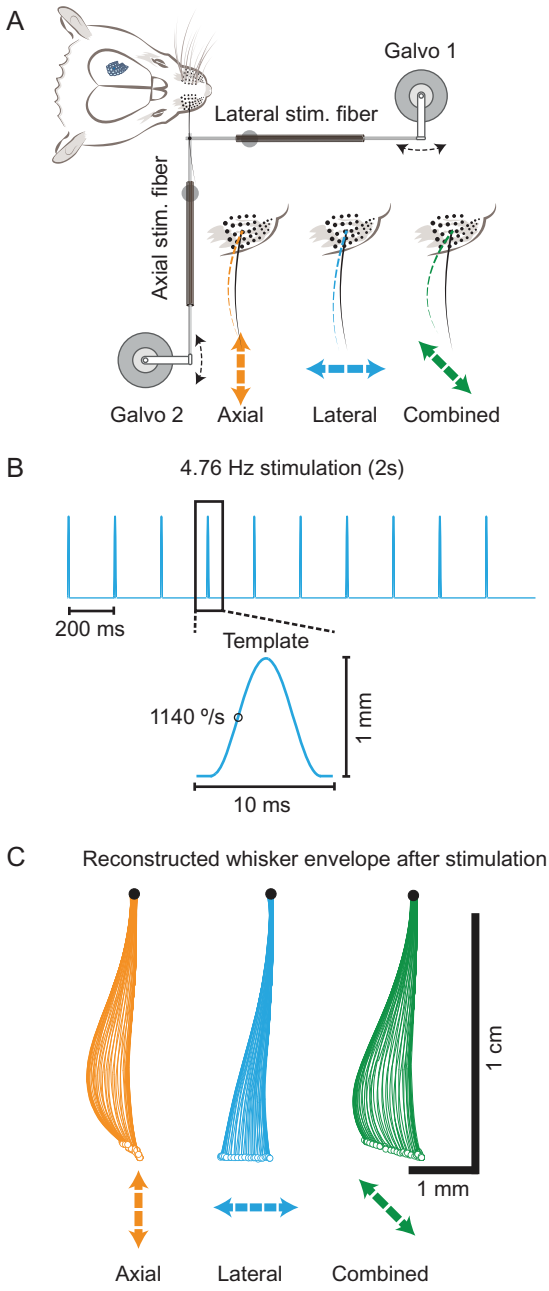

Figure 2. Galvanometer-driven whisker stimulator. (*A*) Axial and lateral whisker stimulation using a pair of optical fibers, each controlled by a galvanometric unit. The fiber tips were attached to the whisker at 1 cm distance from the skin with repositionable glue. Fibers were attached in orthogonal directions to induce axial, lateral, or combined movement of the whiskers. All other whiskers were trimmed to avoid contact with the stimulation fibers. (*B*) For stimulation, we used a phase-shifted 100 Hz cosine template waveform presented at 4.76 Hz repetition rate with 200 ms inter-stimulus intervals. (*C*) Stimulus-induced whisker trajectory after one axial, lateral, or combined stimulation pulse reconstructed from high-speed videography in vivo. Note that the horizontal and vertical axes are scaled 2:1 for visualization of the stimulus-induced whisker envelopes.

In Vivo High-Density Multi-Electrode Recordings

Neural activity was recorded with an 80-channel "silicon probe" inserted perpendicularly into barrel cortex (NeuroNexus Technologies, Ann Arbor, MI, USA). Each of the 4 shanks (3 mm

long) contained 20 recording sites (413 μm^2 surface area per recording site) spaced 50 μm apart. Distance between shanks was 150 μm. Insertion of the probe was guided by intrinsic optical imaging. For each animal, the probe insertion points were marked by impregnating the probes with DiI (1,1′-dioctadecyl-3,3,3′3′-tetramethylindocarbocyanine, Molecular Probes, Eugene, OR, USA) before insertion. A silver wire placed over the cerebellum served as a ground electrode. All data were continuously digitized at 20 kHz and stored for offline analysis using a 256-channel extracellular recording system and MC_RACK software (Multi Channel Systems, Reutlingen, Germany). The total duration of multi-electrode recordings varied between 3 and 5 h.

In Vivo 2-Photon Calcium Imaging

Neuronal ensembles in superficial layers of the principal whisker barrel field mapped by intrinsic signal imaging were bolus-loaded with the AM ester form of Oregon Green BAPTA-1 by pressure injection (OGB-1; 1 mM solution in calcium-free Ringer's solution; 2-min injection at 150–200 μm depth) as described previously (Stosiek et al. 2003). Astrocytes were labeled by surface application of 100 μM Sulforhodamine-101 (5 min incubation time followed by washing of surface area with Ringer's solution (Nimmerjahn et al. 2004). The craniotomy was then filled with agarose (Type III-A, 1% in Ringer's solution; Sigma) and covered with an immobilized glass plate. Two-photon calcium imaging was performed with a custom-built 2-photon laser-scanning microscope 1 h after bolus loading. In vivo imaging was performed with a Ti:sapphire laser system at 840 nm excitation (Mai Tai Deep See; ~120 fs laser pulses). Fluorescence images of 100 × 100 pixels at 10 Hz were collected with a 16× water-immersion objective lens (Nikon, NA 0.8). Data acquisition was controlled by HelioScan (Langer et al. 2013). Duration of calcium imaging recordings varied between 3 and 4 h.

Electrophysiology Analysis

Analysis of Local Field Potential Adaptation by Discrete Fourier Transformation

Local field potential (LFP) traces were first corrected for variations in baseline voltage levels by applying a detrending polynomial fit after low-pass filtering (1–300 Hz) of the continuously digitized recorded data. Next, the LFP response after the first stimulation pulse was used to generate a simulated LFP trace consisting of 10 subsequent whisker-evoked LFP signals. A discrete fast Fourier transform was applied to the simulated and measured LFP data. Ratios of the peaks at the stimulation frequency were calculated as adaptation ratio indices as a measure of response adaptation (Katz et al. 2006).

Current-Source Density Maps

We assessed the cortical depth of individual multi-electrode recordings from stereotaxically estimated depth of insertion as well as vertical current-source density maps (CSD) computed from LFP profiles. The early CSD sinks present after sensory stimulation at the thalamo-recipient L4 and the border between L5 and L6 were used to assign individual channels to specific cortical layers (Mitzdorf 1985). To this end, CSD maps were computed by using the average LFPs of up to 20 trials as described previously (Nicholson and Freeman 1975; Reyes-Puerta et al. 2015). The computed data where then interpolated and visualized as pseudocolor images, with current sources and sinks represented by red (positive) and blue (negative) colors, respectively.

Spike Detection and Sorting

Multichannel-based spike detection and sorting was performed as described previously (Reyes-Puerta et al. 2015). After high-pass filtering (0.8–5 kHz) of the continuously digitized recorded data, non-overlapping groups of 2–4 recording sites were defined as "virtual tetrodes" and processed separately (Harris et al. 2000; Einevoll et al. 2012). Spike detection was performed in each group independently and separately using amplitude-thresholding in the negative range (–7.5 times the standard deviation (SD) of the signal; Gray et al. 1995). Upon threshold crossing on either of the cannels within a group, all sampled amplitude values for all channels in a time range of –0.5 to +0.5 ms relative to the waveform negative peak were extracted. These spike waveforms were then used to compute feature vectors, each containing the negative peak amplitude and 2 first principal components derived from the waveforms. The feature vectors were then used to perform spike sorting (Harris et al. 2000; Hazan et al. 2006). We established several criteria in order to ensure the isolation quality of the sorted neurons, accounting for (1) a clear refractory period existing in the overall activity of the isolated units, (2) a stable spontaneous firing rate during the whole recording period, and (3) a valid "isolation distance" obtained in the spike sorting procedure (for further details see Reyes-Puerta et al. 2015).

Cells were subsequently classified as putative excitatory (EXC) pyramidal neurons and putative inhibitory (INH) interneurons based on their mean spike waveform. For each neuron 2 parameters were calculated, which have been shown to reliably separate between the 2 identified neuronal populations in adult rodents in vivo (Guo et al. 2014; Reyes-Puerta et al. 2015): (1) the onset to (late) peak latency, and (2) the asymmetry index. This procedure was successful in separating between 2 neuronal classes in the P17–P28 age group. However, no separation could be obtained in any of the younger age groups (P10–P12 and P13–P16), in which no INH neuron clusters could be reliably separated. These data are in agreement with the finding that different types of fast spiking INH neurons show only fully matured spike waveform profiles from ~P15 onwards (Doischer et al. 2008).

Spike trains were represented as spike rasters and peristimulus time histograms using 1-ms time bins for MUA data and 10-ms time bins for single-unit activity (SUA) data. For each pulse during the 2-s stimulation, sensory-evoked responses were evaluated by quantifying spike counts within the first 50 ms after pulse onset ("early" time window) and within a 50–150 ms time window ("late" response). Average firing rates were represented by mean ± s.e.m. of 20 trials. Baseline activity was calculated as the average spike rate 100 ms before presenting the 10 successive pulses. The slope of the decay of the mean sensory-evoked MUA responses 100–200 ms after each stimulation pulse was obtained by a linear regression fit. Data analysis of spike trains was performed in MATLAB.

Detection of Sensory-Evoked Response Latencies

Response latencies after whisker stimulation were computed for different layers from smoothed MUA recordings from a specific recording site closest to the identified layer (convolution of a Gaussian window filter, 5 ms). First, the peak MUA response was identified in a 50 ms window after stimulation. Second, the mean base response 100 ms before stimulation was calculated. Response onset was identified if (1) the response was bigger or equal to the mean base response and smaller than 3 SDs of the peak response. Onset detection was also performed on spike-

sorted data by detection of the first spike occurring in each of the 20 trials in a 50 ms window after stimulation. Both, the detected MUA and SU response latencies showed similar response latencies.

Assignment of Recording Sites to Cortical Layers

Differences in cortical thickness across developmental age groups were normalized by choosing a fixed number of recording sites per cortical layer (not exceeding layer thickness in the P10–12 age group). Recording sites fully embedded in the corresponding layers, as revealed by the CSD maps, were used as reference points to annotate additional recording sites. The number of recording sites per animal was kept constant for all layers and age groups (L2/3: 1; L4: 2; L5: 2; L6: 2).

Analysis of Calcium Imaging Data

Calcium imaging data were imported and analyzed using routines custom-written in NIH ImageJ and MATLAB. First, fluorescence image time-series for a given region were concatenated. The concatenated imaging data was then aligned using TurboReg to correct for small x-y drift (alignment on SR-101 channel, transferred to OGB-1 images, NIH ImageJ; Thévenaz et al. 1998). As a next step, background was subtracted as the bottom first percentile fluorescence signal of the entire image. Average intensity projections of the imaging data were used as reference images to manually annotate regions of interest (ROIs) corresponding to individual neurons. Neurons with somata partly out-of-focus were not included. Calcium signals were expressed as the mean pixel value of the relative fluorescence change $\Delta F/F = (F–F_0)/F_0$ in a given ROI. F_0 was calculated as the bottom 10th percentile of the fluorescence trace. The neuropil signal was defined by all pixels not assigned to a neuronal soma or astrocyte of the overall ROI annotation. Active neurons were identified by 2-way ANOVA of the evoked neuropil and neuronal signal (significance value $P < 0.05$). Stimulus-responsive neurons were identified by 2-way ANOVA of pre- and post-stimulus time periods (significance value $P < 0.05$). For each stimulus the evoked responses of 20 trials were analyzed and the response magnitude expressed as the mean of the evoked ΔF/F integral (%·s; integral of response for the 2-s stimulation window). This metric compensates for possible differences in calcium transient dynamics and cellular calcium buffering in different age groups and animals. Pearson's correlation coefficients of spontaneous and sensory-evoked responses for 2 neurons at zero lag were calculated between pairs of somatic calcium traces (60 s spontaneous data; mean of 20 × 2 s evoked data). Regression lines fitted to scatter distributions of different age groups were compared for statistical difference by performing a 2-tailed *t*-test. Two regression lines were considered to be significantly different if the student's *t*-distribution functions of the underlying scatter distribution pairs were significantly different.

Analysis of Response Selectivity

For each single unit, the response selectivity index was defined as the area under the receiver operating characteristic curve (auROC) based on the average firing rate during the initial 50 ms after each stimulation pulse for 20 trials per stimulus type. Differences in response selectivity distributions were analyzed using the nonparametric Kolmogorov–Smirnov test where each empirical function was represented as the cumulative distribution of auROC across age groups.

For the in vivo 2-photon calcium imaging data, auROC was calculated for each ROI using the means of the evoked ΔF/F integral (in %·s units) for preferred (μ_p) or non-preferred (μ_{np}) stimulus with the preferred stimulus defined by the larger mean ΔF/F integral for either axial or lateral stimulation ($\mu_p > \mu_{np}$). This approach results in auROC values ranging from 0.5 (no selectivity) to 1.0 (perfect selectivity for preferred stimulus).

Statistical Analysis

Data are represented as mean ± s.e.m. unless stated otherwise. One- or two-way ANOVA was used to test for significance for normally distributed data, followed by post hoc Tukey's test. The Kruskal–Wallis test was used for non-normally distributed data, followed by Dunn–Sidak's post hoc test. Significance threshold was set to $P < 0.05$; in the figures, different degrees of evidence against the null hypothesis are indicated by asterisks ($^*P < 0.05$; $^{**}P < 0.01$; $^{***}P < 0.001$).

Results

Onset of Locomotion and Whisking Behavior in the Third Postnatal Week

We first identified the developmental period during which mice show prominent behavioral changes related to processing of whisker information. We analyzed explorative behavior in an open field test between P10 and P28 (Fig. 1*A* and Supplementary Movie 1). Before P13, mice were rather immobile and showed minimal active whisking. Around P14, shortly after eye opening, mice began to exhibit rhythmic active whisking and displayed a significant increase in travel distance (Fig. 1*B* to *D*). In parallel, the fraction of time spent actively whisking against the wall increased (Fig. 1*E* and *F*). This marked behavioral change occurred within a short time window between P13 and P16, coinciding with the critical developmental period of L2/3 in barrel cortex (Stern et al. 2001), with little changes thereafter. Similar results have been previously reported for both rats (Landers and Philip Zeigler 2006; Grant et al. 2012) and mice (Arakawa and Erzurumlu 2015). Importantly, enhanced whisking activity and a higher incidence of touches will result in a net increase of both lateral and axial forces impinging on the whisker follicle and, thus, the tactile receptors (Ebara et al. 2002). These changes in experience likely are associated with changes in cortical processing of whisker stimuli. We therefore aimed to analyze sensory-evoked activity in barrel cortex using controlled whisker stimulation across 3 age groups: before eye opening and whisking onset (P10–P12), during the critical period (P13–P16), and afterwards (P17–P28).

A Novel Galvanometer-Driven Stimulator for Precise Whisker Control

To apply axial and lateral forces independently or in combination to an individual whisker, we developed a galvanometer-driven stimulator. The stimulator consists of 2 optical fibers orthogonally glued together near their tips, attaching them to a single whisker (Fig. 2*A*; see also Methods and Supplementary Fig. S1). Our stimulation protocol consisted of 10 successive single-whisker stimuli delivered at 4.76 Hz (Fig. 2*B*; 10-ms stimulus waveform plus 200-ms inter-stimulus interval, 1 mm amplitude at 10 mm distance from the snout; deflections applied axially, laterally, or in combination). Axial forces

pushed the whisker into the follicle whereas lateral forces deflected the whisker in the anterior–posterior direction (Fig. 2C), similar to standard whisker deflection experiments using piezoelectric devices (Simons 1983). Induced whisker movements displayed high spatial and temporal precision with little deviation from the desired waveform across all age groups and negligible after-oscillations (Supplementary Fig. S1 and Supplementary Movie 2). This stimulator enabled us to study the developmental profile of sensory-evoked neuronal responses as well as their selectivity for axial or lateral stimulation, using in vivo multi-electrode recordings and 2-photon calcium imaging in lightly urethane-anesthetized mice.

Layer-Specific Intra-Columnar Development of Whisker-Evoked Activity

We first asked whether the representation of whisker stimuli changes across cortical layers in the 3 defined age groups. We used 80-channel multi-electrode arrays (4 shanks spaced 150 μm apart; 20 linearly arranged electrodes per shank, 50 μm inter-electrode distance) and measured LFPs, multi-unit activity (MUA), and SUA in identified barrel columns across all cortical layers (Fig. 3). Electrodes were covered with DiI and for each experiment we identified the exact electrode position by visualizing the DiI traces of the shank insertion points (see also Supplementary Fig. S2). We calculated CSD maps from the LFPs to assign recording electrodes to individual barrel-related columns and cortical layers (Fig. 3). At all ages, L4 could be identified by the prominent current sinks occurring shortly after whisker stimulation (response onset latency for P10–12: 20.3 ± 0.3 ms; P13–16: 17.1 ± 0.3 ms; P17–28: 15.3 ± 0.4 ms; mean ± s.e.m., $n = 6$ mice per age group). In agreement with previous work (Mitzdorf 1985; Reyes-Puerta et al. 2015), activity subsequently propagated towards L2/3 as indicated by slightly longer onset latencies in L2/3 (P10–12: 22.2 ± 0.3 ms; P13–16: 19.0 ± 0.3 ms; P17–28: 16.5 ± 0.3 ms; $n = 6$ mice per age group). We could thus reliably identify cortical layers in the recorded barrel columns at different developmental time points. In animals younger than P12, sensory-evoked LFP responses were mainly confined to L2/3 and L4 of the barrel column corresponding to the stimulated whisker (Fig. 3A, typical example of a P11 animal). Only small-amplitude LFP responses were apparent in L5 and L6 (with an early CSD sink in upper L6), which strongly adapted following the first stimulus. In contrast, older animals displayed larger-amplitude LFP responses with little adaptation also in deeper layers (Fig. 3C; representative example of a P26 animal from the P17–28 age group). These changes in adaptation of LFP responses were significant across age groups (Supplementary Fig. S3).

We further examined layer-specific developmental changes of sensory-evoked responses by analyzing MUA across cortical layers (Fig. 4). Mean evoked spike rates significantly decreased with age in L2/3 and L4 but increased in L5 and L6 (Fig. 4A,B). Interestingly, spontaneous spiking activity showed a similar developmental increase in the deeper layers (Supplementary Fig. S4). To quantify changes in response adaptation across development, we compared the ratio of response integrals for the last versus the first stimulation pulse. In addition, we subdivided the MUA profiles into an early (0–50 ms) and a late (50–150 ms) response window after the respective stimulation pulses. In L2/3 and L4, early MUA response ratios were above 100% in young animals (indicating facilitation) and then significantly decreased with age (Fig. 4C). In contrast, neurons in L5 displayed response ratios below 100% in the youngest age group (indicating adaptation), which then increased with age. Thus, at a stimulation frequency of ~5 Hz early-evoked spiking activity in lightly anesthetized mice effectively converges in all layers towards little adaptation in the postnatal development period investigated here. Distinct developmental profiles for superficial versus deeper layers were also observed for the response ratios of spiking integrals in the late temporal window (50–150 ms), which relate to evoked circuit reverberations. Whereas late response ratios significantly decreased in L2/3 and L4 during postnatal development, they increased in L5 and L6 (Fig. 4D). We obtained similar results for lateral whisker stimulation (Supplementary Fig. S5). We further analyzed the kinetics of the sensory-evoked late response component by fitting a line to it. The slope of this line became significantly more negative in all layers except L6 between P10–12 versus P17–28 age groups (L2/3: −71.8 ± 43.5 vs. −300.1 ± 51.1, $P = 0.008$; L4: −63.9 ± 91 vs. −487.4 ± 106.6, $P = 0.012$; L5: −148.8 ± 35.5 vs. −424.1 ± 82.4, $P = 0.004$; L6: −132.8 ± 23.3 vs. −285.5 ± 50.5, $P = 0.08$; units of spikes/s^2).

In general, axial or lateral whisker stimulation showed similar response profiles at the MUA level. Together, these findings demonstrate that both sensory-driven cortical activation patterns and the resulting spiking activity undergo in parallel prominent and layer-specific changes at the onset of exploratory locomotion behavior during the third postnatal week.

Layer-Specific Cross-Columnar Development of Whisker-Evoked Activity

We further studied the development of lateral spread of activity across neighboring barrel columns. We compared sensory-evoked MUA in the principal whisker-column with its neighboring column (Fig. 5A). Mean spike rates in L2/3 and L4 of the neighboring column, when normalized to the principal column, significantly increased with age for both axial (Fig. 5B) and lateral (Fig. 5C) stimuli. No clear change was found in L5 and L6, although a non-significant similar trend was visible. We conclude that during postnatal maturation, in addition to an intra-columnar layer-specific refinement, cross-columnar spread of whisker-evoked activity becomes larger, especially in L2/3 and L4.

Emerging Response Selectivity for Axial or Lateral Whisker Stimuli

Next, we addressed the question whether exertion of axial or lateral whisker forces elicits distinctive responses in single neurons. To analyze selectivity of neuronal responses at the single-unit (SU) level we performed multichannel spike sorting and isolated a total of 737 SUs in 15 animals ($n = 5$ animals per age group; P10–12: 236 SUs, P13–16: 254 SUs, P17–28: 247 SUs; see Methods and Supplementary Fig. S6). We assigned the isolated SUs to the recording site (and the corresponding cortical layer), for which the waveform amplitude was maximal (Fig. 6A). Furthermore, in the P17–28 age group we could discriminate putative excitatory (EXC) from putative inhibitory (INH) SUs based on their waveform asymmetry and spike width (Fig. 6B). We identified a proportion of 22.7% putative INH SUs (56 out of 247 units) consistent with previous studies (Sakata and Harris 2009; Reyes-Puerta et al. 2015). For the younger age groups, discrimination of EXC and INH SUs was not feasible because waveform features were not sufficiently distinct (Methods and Supplementary Fig. S6).

We quantified the response selectivity for axial or lateral stimulation using the area under the receiver operating

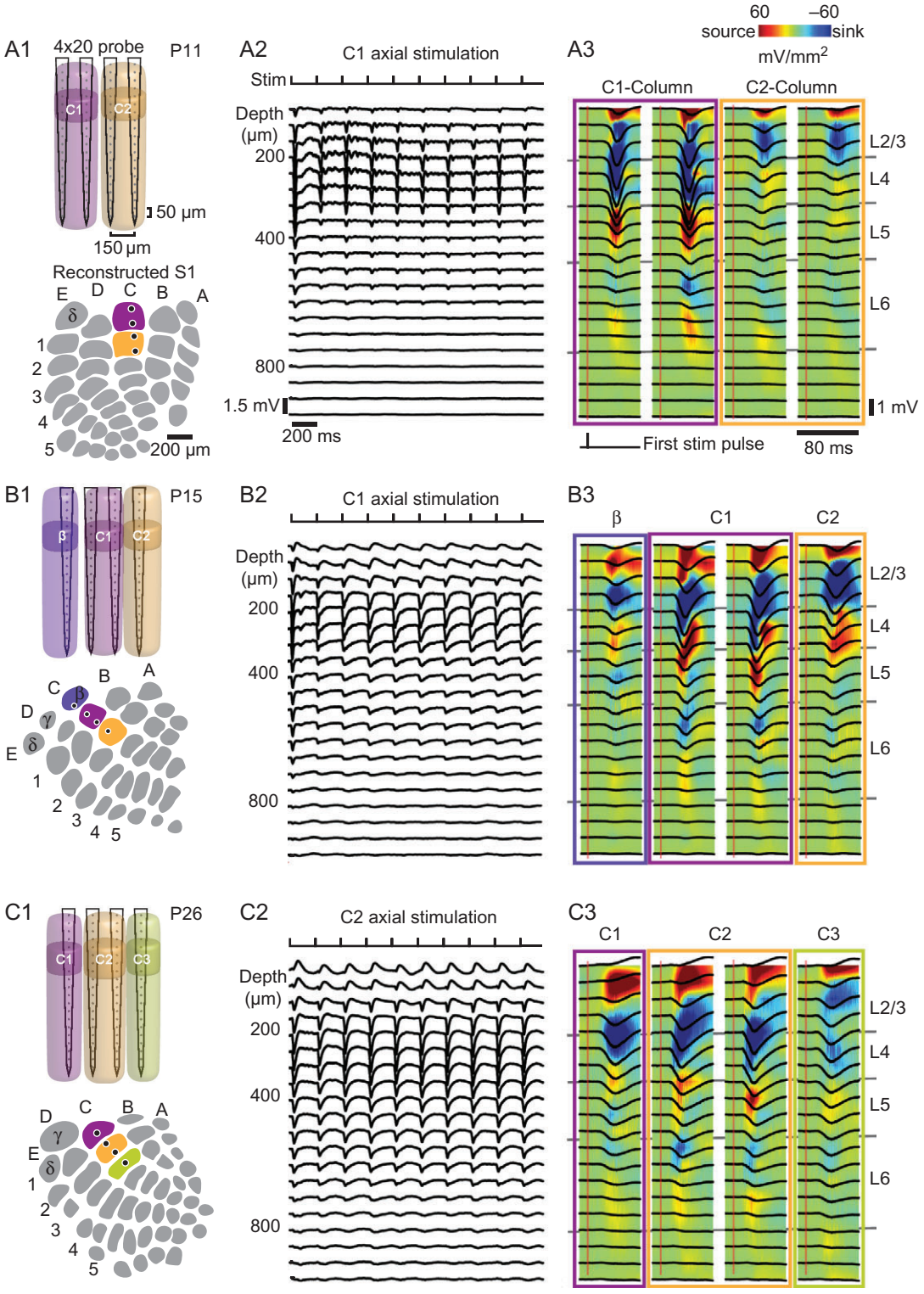

Figure 3. Multi-electrode array recordings of single-whisker evoked cortical activity. (*A*) Example recording of a P11 mouse. (*A1*) Schematic of multi-electrode array placement. For all animals, the array was inserted perpendicular to the C1 and C2 barrel columns (with small variations in relation to the barrel field). (*A2*) LFPs evoked by axial whisker stimulation (average of 20 trials). (*A3*) CSD maps computed from the first stimulation pulse of the 4.76 Hz stimulation (average of 20 trials). Sinks are indicated by blue and sources by red colors. Borders of cortical layers were identified from the CSD maps and stimulus onset times, indicated as grey traces in the background. Vertical red lines indicate stimulus onset. (*B*) and (*C*) Examples of multi-electrode array position, LFPs and CSD maps in a P15 and P26 mouse, respectively (same conventions as in *A*).

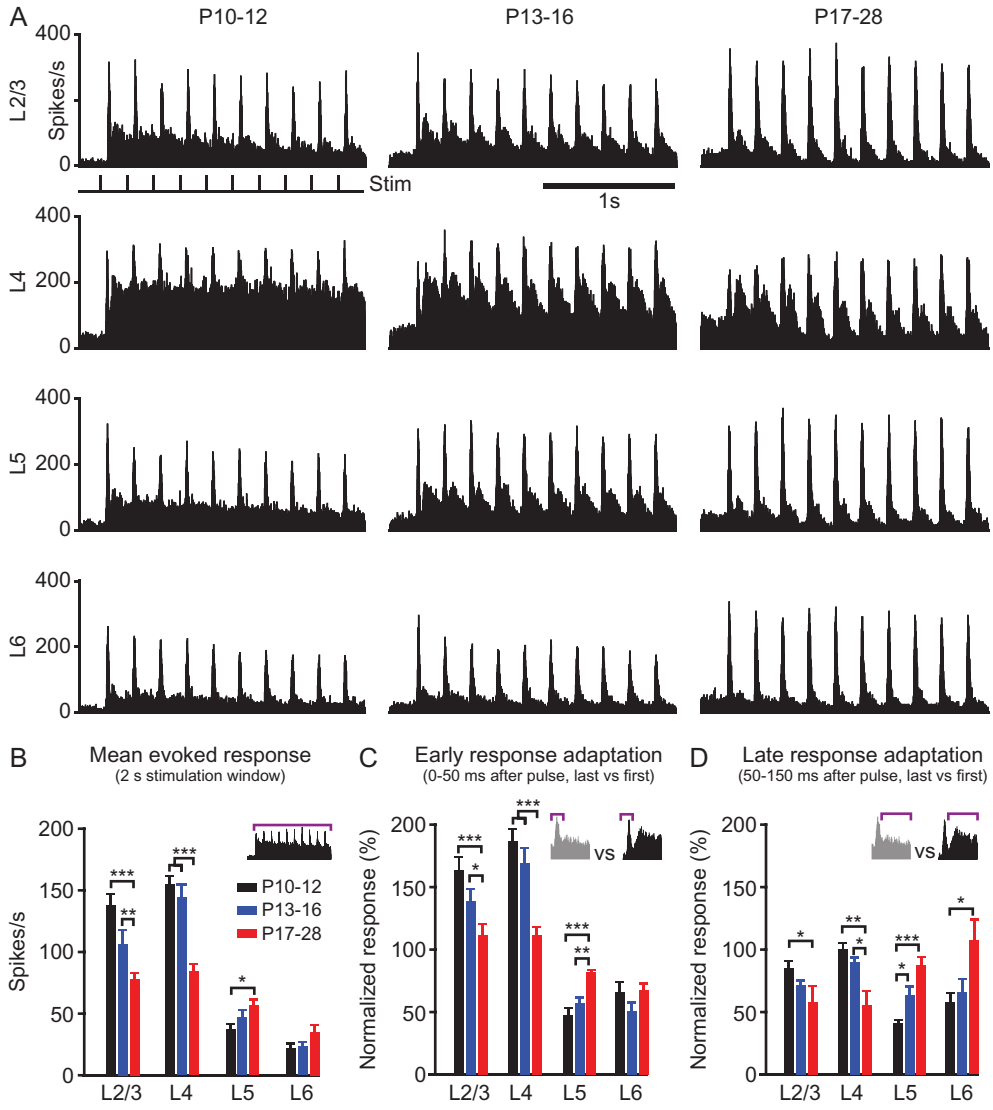

Figure 4. Intra-columnar development of sensory-evoked activity. (*A*) Pooled average MUA across cortical layers and age groups (examples show responses to axial stimulation, see also Supplementary Fig. S5 for lateral responses). For each animal, we selected 4 representative electrodes corresponding to superficial L2/3 and the centers of L4, L5, and L6 for the analysis. (*B*) Pooled analysis of the mean evoked response (2 s) for all cortical layers and age groups. (*C*) Quantification of early response adaptation (spike counts 0–50 ms after stimulation pulse). Normalized responses indicate the ratio for the last versus first stimulation pulse. (*D*) Quantification of late response adaptation (normalized spike count in 50–150 ms window for last vs. first stimulation pulse). Data points are mean ± s.e.m. (n = 18 mice, 6 mice per age group). Statistics: Kruskal–Wallis test followed by Dunn–Sidak's post hoc correction (*P < 0.05, **P < 0.01, ***P < 0.001).

characteristic (auROC; see Methods). We based the calculation of auROC on spike count distributions for axial and lateral stimulus-evoked responses obtained within the first 50-ms window following each stimulation pulse. SUs showed diverse response selectivity to the presented stimuli (Fig. 6*C*,*D*). In the P10–12 age group, SUs generally responded with low selectivity (auROC < 0.8) whereas in the older age groups, we observed an up to 3-fold increase from pre- to post-critical period in the fraction of SUs with auROC > 0.8: (P10–12: 8%, P13–16: 18%, P17–28: 24% of SUs across all layers). Based on the cumulative distributions of auROC indices, this increase in selectivity reached significance for SUs in both L5 and in L6 (Fig. 6*E*). INH SUs displayed high diversity in response selectivity and response strength, comprising highly responsive and selective as well as low responsive and unselective INH SUs (indicated in red in Fig. 6*D*). Scatter distribution analysis of axial and lateral responses showed an increase in preference to axial stimulation for L5 and L6 (Supplementary Fig. S7). For the combined stimulus, responsive SUs typically showed a similar response pattern as for the preferred stimulus, although some neurons responded little to combined stimulation (Fig. 6*C*, SU example in P14 animal). These findings present evidence for emerging response selectivity in the developing barrel cortex circuitry in L5 and L6 during the same period when active whisking and explorative behavior mature.

Refinement of Sensory-Evoked Activity in L2/3 Neurons

To corroborate these findings for the L2/3 critical period and in order to examine developmental changes in the L2/3 cortical representation of whisker-evoked activity more comprehensively, we performed in vivo 2-photon calcium imaging across the same 3 age groups. Following bulk loading of L2/3 with the synthetic calcium indicator Oregon Green BAPTA-1 (OGB-1; see

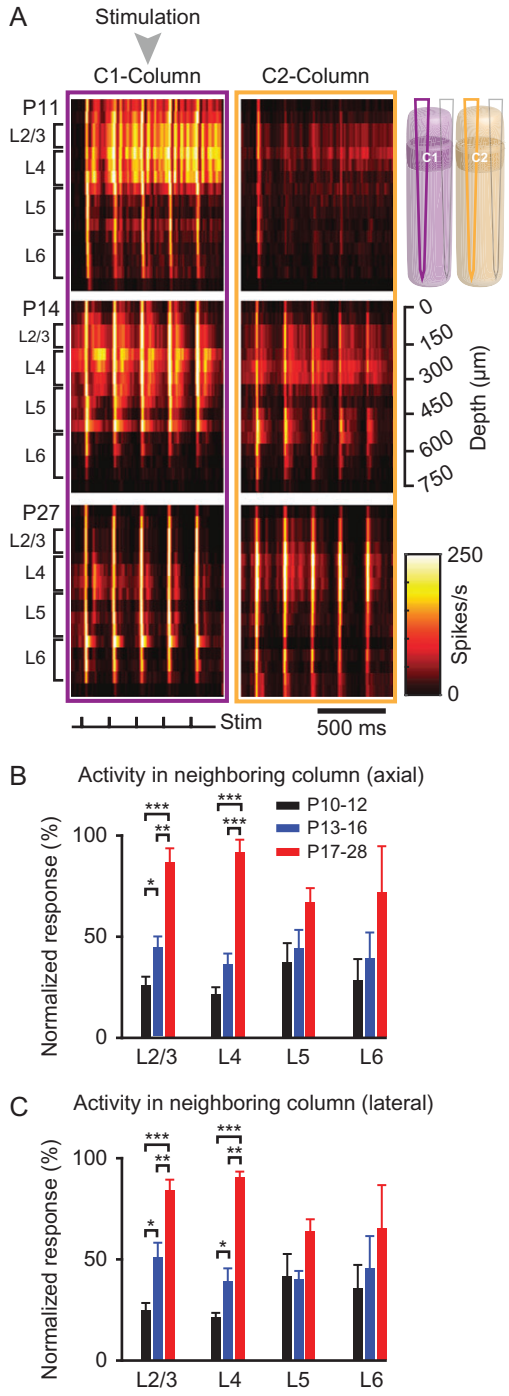

Figure 5. Cross-columnar development of sensory-evoked activity. (*A*) Heatmap showing MUA in the principal (C1) and neighboring (C2) barrel column after axial stimulation of the C1 whisker. Examples from a P11, P14, and P27 mouse. Responses to the first 5 stimulation pulses are shown (colorbar, black: 0 spikes/s; white: 250 spikes/s). (*B*) Quantification of the sensory-evoked activity in the neighboring barrel column normalized to the principal barrel column firing rate for axial stimulation. (*C*) Quantification of cross-columnar activity for lateral stimulation. Same conventions as in (*B*). Data points are mean ± s.e.m. (n = 18 mice, 6 mice per age group). Statistics: Kruskal–Wallis test followed by Dunn–Sidak's post hoc correction (*$P < 0.05$, **$P < 0.01$, ***$P < 0.001$).

Methods) we imaged a large number of L2/3 neurons with high spatial resolution (Fig. 7A; 2709 cells in n = 18 mice; compared with 74 SUs in n = 15 mice isolated in L2/3 of which 61 were used for response selectivity analysis). Both spontaneous and evoked population activity transitioned from highly synchronized and large calcium transients before P13 to decorrelated and sparser calcium transients at older ages (Fig. 7*B*,*C*). This sparsification and decorrelation was most obvious in the pooled analysis of evoked ΔF/F integrals and of pairwise neuronal correlations for the P13–16 age group for both spontaneous and evoked activity (Fig. 7*D*,*E*). The proportion of neurons responding to a given stimulus decreased more than 2-fold between the P10–12 and P17–28 groups indicating sparsification of overall responsiveness in L2/3 (Fig. 7*F*). Thus, consistent with our results from MUA analysis, we conclude that responsiveness decreases in superficial L2/3, paralleled by decorrelation of spontaneous and sensory-evoked network activity in the critical period.

Emerging Response Selectivity in L2/3

We also analyzed whether populations of L2/3 neurons increase their response selectivity for axial or lateral whisker stimulation across development, as indicated by the SU responses. Indeed, while overall decreasing their responsiveness, neurons displayed increasing response selectivity for either axial (Fig. 8*A*) or lateral stimulation (Fig. 8*D*). Populations of neurons preferably responding to axial stimulation showed a significantly higher fraction of axial-selective neurons for the P13–16 and P17–28 age group compared with the P10–12 age group (Fig. 8*B*,*C*). This increase in response selectivity across development was also significant for neurons selective to lateral stimulation (Fig. 8*E*,*F*). Neurons selective for either axial or lateral stimulation were detectable simultaneously in local populations of L2/3 networks around P14 (Supplementary Fig. S8). These results provide further evidence for specific changes in whisker-evoked L2/3 neuronal dynamics in developing barrel cortex, with a reduction in response amplitude, along with an increase in response selectivity for axial and lateral whisker forces following the onset of active explorative behavior.

Finally, we evaluated how L2/3 neuronal responses to combined axial-lateral stimulation related to the individual component responses across development. Albeit individual neurons showed heterogeneous summation of axial/lateral responses (with a few neurons showing supra-linear responses), L2/3 populations on average responded to combined stimulation in a sublinear manner. This effect was significantly more pronounced in the older age groups (Fig. 9; scatter distributions from 6 animals per age group; P10–12 vs. P13–16, P = 0.00001; P10–12 vs. P17–28, P = 0.012; analysis of regressions slopes, see Methods). This result was corroborated by analyzing only the subsets of neurons showing highest selectivity for either axial or lateral stimulation. Sublinear regression distributions for both the axial- and lateral-selective neuronal subsets showed similar distributions as the grand population average (Fig. 9). With increasing age, especially axial-selective neurons exhibited a significant reduction in response summation for the combined whisker stimulus (P10–12 vs. P17–28, P = 0.0027). Together, these findings suggest that when mice start explorative behavior, activation of cortical neurons by axial and lateral whisker force components experiences enhanced competition, possibly because of increased cortical inhibition, which could contribute to the emerging response selectivity.

Discussion

In summary, we have characterized the developmental profile of sensory-evoked activity in barrel cortex of mice between P10

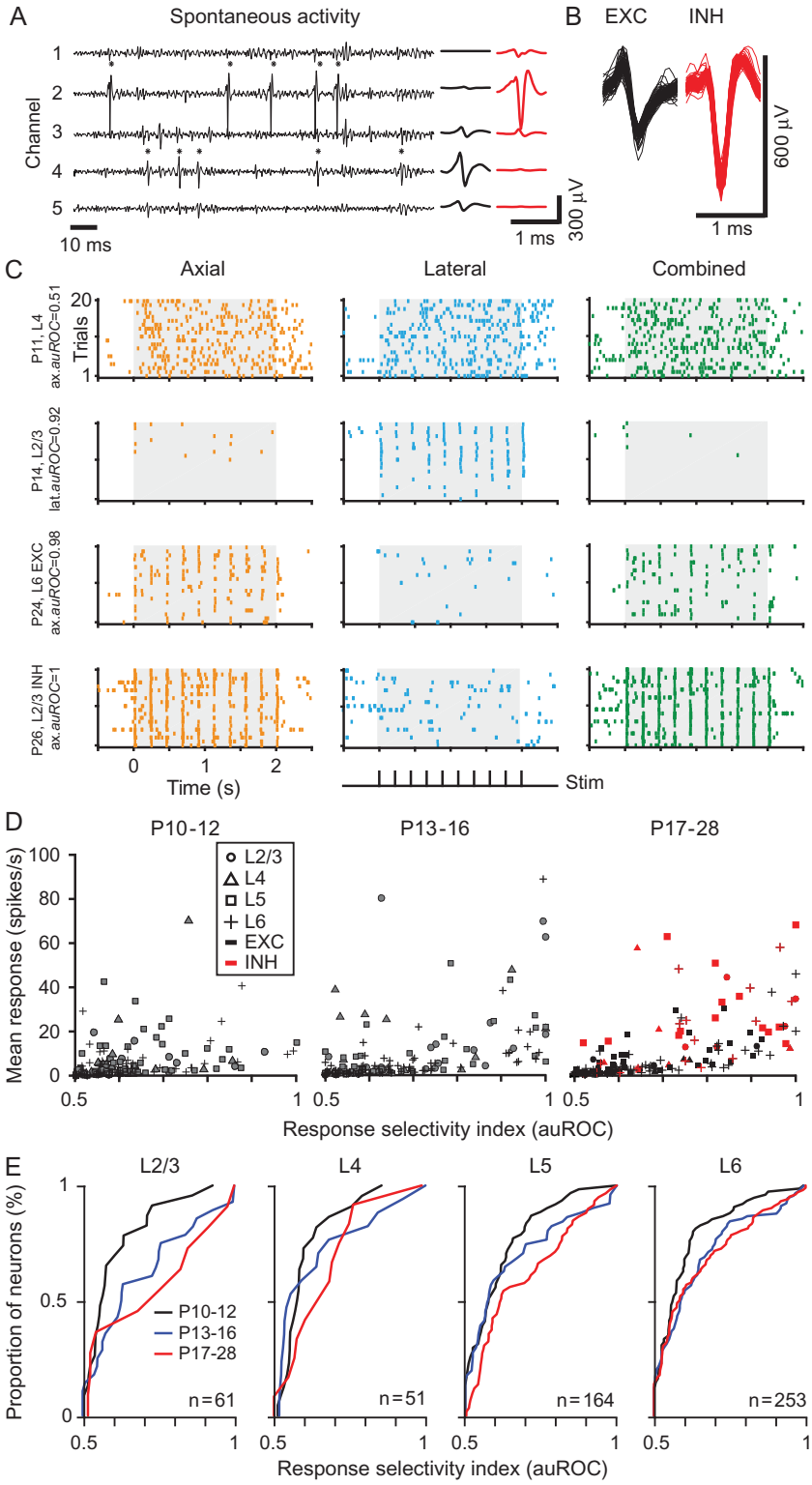

Figure 6. Development of single-unit response selectivity. (*A*) Left: High-pass filtered signals (0.8–5 kHz) from 5 contiguous channels containing 90 ms of spontaneous activity. Black stars indicate time points at which spikes were detected and sorted (see also Supplementary Fig. S6). Right: Average spike profiles of 2 isolated SUs. (*B*) Spike waveforms extracted from the channel with the highest negative peak as shown in (*A*) for a putative excitatory (EXC) and a fast-spiking, putative inhibitory (INH) cell. (*C*) Spike-raster plots of sensory-evoked activity for all stimuli in a P11, P14, P24, and P26 mouse. Grey boxes indicate whisker stimulation. Examples show nonselective (P11) and selective (P14, P24, P26) examples. (*D*) Pooled analysis of response selectivity index (auROC) of SUs located in the barrel column of the stimulated whisker. Data points indicate auROC for single SUs and layer identity. In the P17–28 age group, SUs are labeled as EXC (black) or INH (red) based on waveform clustering (as seen in B). (*E*) Cumulative distribution analysis of the response selectivity index (auROC) across cortical layers and age groups ($n = 5$ animals per age group). Kolmogorov–Smirnov test; *P*-values for P10–12 versus P13–16: [0.15, 0.18, 0.61, 0.03] for L2/3, L4, L5, L6, respectively; for P10–12 versus P17–28: [0.06, 0.12, 0.02, 0.04]; for P13–16 versus P17–28 [0.59, 0.18, 0.13, 0.87]; number of analyzed cells for P10–12: [23,22,57,72] for L2/3, L4, L5, and L6, respectively; P13–16: [27,17,48,85]; P17–28: [11,12,59,96].

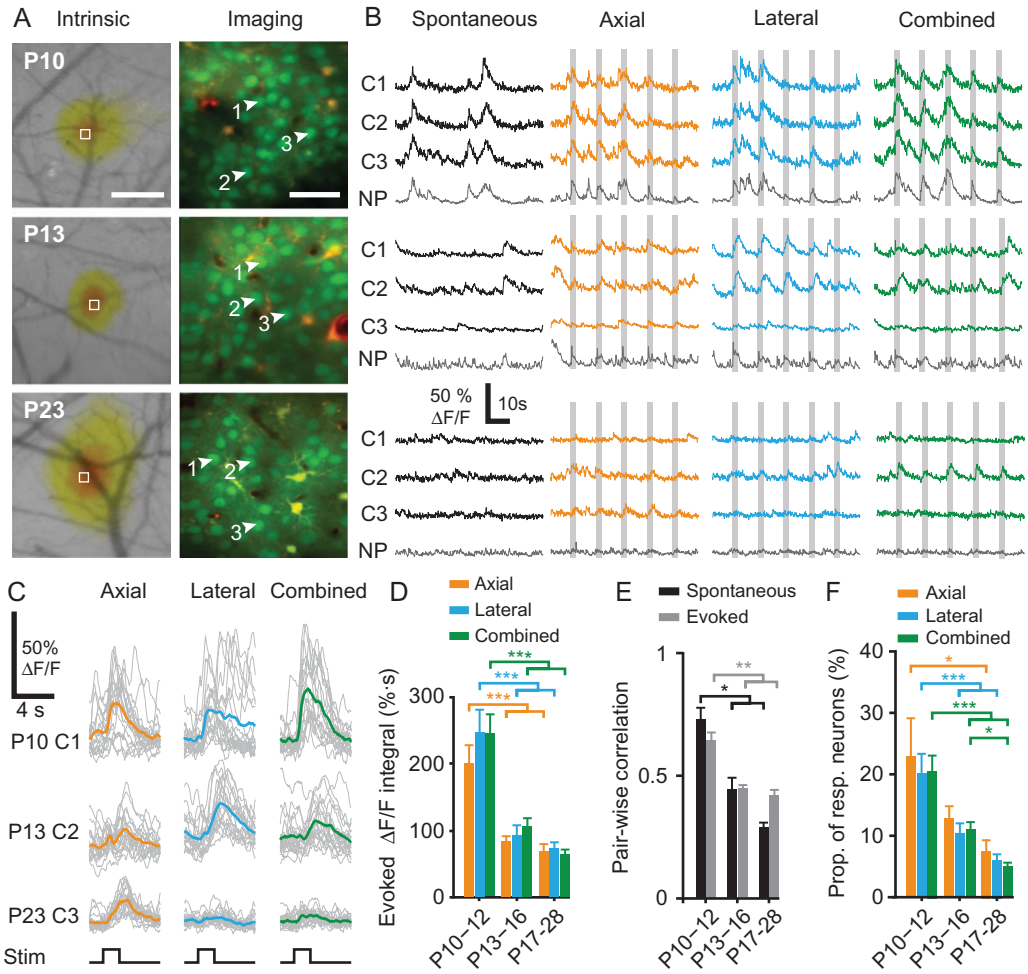

Figure 7. Stimulus-evoked calcium dynamics in layer 2/3 neurons. (*A*) Identification of the C2 barrel using intrinsic optical imaging (left) in a P10, P13, and P23 mouse. Squares indicate imaging regions depicted on the right; Scale bar 250 μm. Right: maximum intensity projections of calcium imaging regions after cell bolus loading of OGB-1 AM (green). Sulforhodamine-101 staining of astrocytes in red; Scale bar 30 μm. (*B*) Raw ΔF/F traces of spontaneous (black) and sensory-evoked activity (color-coded, C1, C2, C3). Bottom grey traces show neuropil signal (NP; see Methods). (*C*) Single trial (grey) and mean (color coded) evoked calcium transients (n = 20 trials per stimulus) for neurons as shown in (B) (P10: neuron 1 (C1), P13: neuron 2 (C2), P23: neuron 3 (C3)). (*D*) Pooled analysis of the evoked response integral for all stimuli in L2/3 (axial, lateral, combined). (*E*) Pooled analysis of pair-wise correlations of spontaneous (black) and sensory-evoked (grey) neuronal activity (n = 3 animals, 320 cells). (*F*) Pooled analysis of proportion of responsive cells for a given stimulus type. Data show means ± s.e.m. (n = 6 animals per age group, 2709 cells). Statistics: Kruskal–Wallis test followed by Dunn–Sidak's post hoc correction (*P < 0.05, **P < 0.01, ***P < 0.001).

and P28, including in particular the short time window around P13 when animals open their eyes and start actively exploring the environment with their whiskers. We found several layer-specific changes in response profiles at the onset of active whisking behavior. First, on the MUA and LFP level, sensory-evoked responses consistently decreased in L2/3 and L4 with age, whereas they increased in L5 and L6, irrespective of the type of stimulation (axial or lateral). Second, superficial and deep layers also differed with respect to neuronal adaptation and its developmental profile: whereas superficial layers showed facilitation before the critical period, which then turned into slight depression, deep layers showed the opposite trend with pronounced adaptation at early age, which then became less prominent in older animals. In addition, analysis of single neuron responses revealed emerging response selectivity for axial or lateral stimuli around P14 for L2/3, L5, and L6. Together, these findings demonstrate that maturation of sensory processing in mouse barrel cortex involves substantial layer-specific changes in a short time-window at the onset of active whisking behavior.

Our results confirm previous findings demonstrating rapid functional changes of barrel cortex activity within only 2–3 days in the critical period around P13. These findings include sparsification and decorrelation of spontaneous L2/3 population activity (Golshani et al. 2009; Ikezoe et al. 2012), sharpening of evoked temporal spiking profiles (Ikezoe et al. 2012), and changes of signal flow across large portions of the cerebral hemispheres (Quairiaux et al. 2011). The aging-related sparsification of spontaneous activity (and of sensory-evoked activity as shown here) can be explained at least in part by changes in intrinsic neuronal properties, especially a pronounced progressive decrease in input resistance (Maravall et al., 2004). Further likely causes are layer-specific changes of synapse density (Chandrasekaran et al. 2015), plasticity-induced changes of L4-to-L2/3 and L2/3-to-L2/3 synaptic connectivity (Stern et al. 2001; Wen and Barth 2011), maturation and pruning of thalamocortical inputs (Yu et al. 2012), and maturation of the inhibitory circuitry (Zhang et al. 2011).

A new finding of our study is the emergence of response selectivity in barrel cortex during the critical period of L2/3

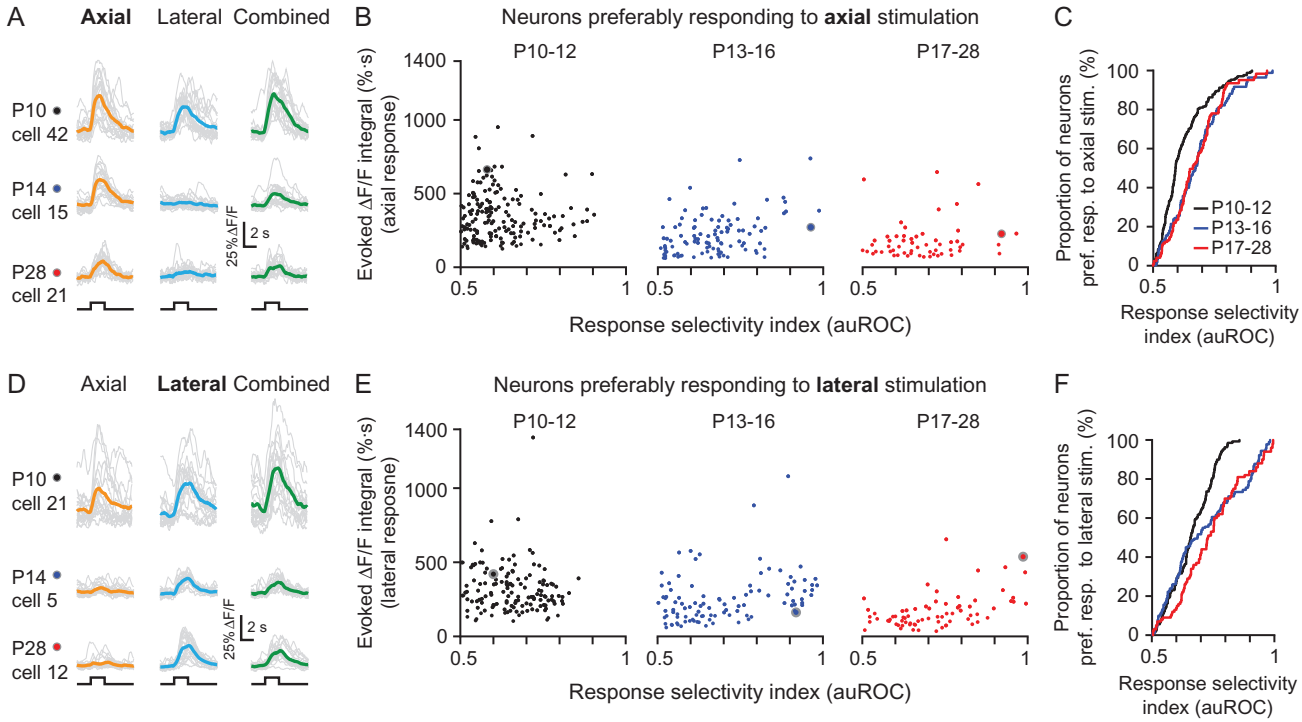

Figure 8. Development of single neuron stimulus-selectivity in L2/3 to either axial or lateral whisker stimulation. (*A*) Single trial (grey) and mean (color-coded) evoked calcium transients (n = 20 trials per stimulus) of neurons preferably responding to axial whisker stimulation. (*B*) Scatter distributions of the response amplitude [expressed as the evoked ΔF/F integral (%·s)] and corresponding response selectivity index auROC (see Methods) for neurons preferably responding to axial whisker stimulation. Position of example neurons of panel (*A*) is indicated. (*C*) Cumulative distribution analysis of response selectivity (auROC) across age groups. The distributions of selectivity to axial stimulation for animals older than P13 were significantly different from young animals (≤P12), since their distributions contained more stimulus-selective cells with higher auROC values. Kolmogorov–Smirnov test; P10–12 versus P13–16: $P = 1.1{\cdot}10^{-10}$; P10–12 versus P17–28: $P = 3.4{\cdot}10^{-11}$; P13–16 versus P17–28: $P = 0.59$; 192, 86, and 54 cells for P10–12, P13–16, and P17–28, respectively; n = 6 animals per age group. (*D*) Example evoked calcium transients of neurons preferably responding to lateral whisker stimulation. Same conventions as in (*A*). (*E*) Scatter distributions of the response amplitude and auROC for neurons preferably responding to lateral whisker stimulation. (*F*) Cumulative distribution analysis of response selectivity (auROC) across age groups. Kolmogorov–Smirnov test; P10–12 versus P13-16: $P = 7.4{\cdot}10^{-9}$; P10–12 versus P17–28: $P = 2.7{\cdot}10^{-7}$; P13–16 versus P17–28: $P = 0.006$; 148, 95, and 69 cells for P10–12, P13–16, and P17–28, respectively; n = 6 animals per age group). Note that auROC values are confined to 0.5–1 (see Methods).

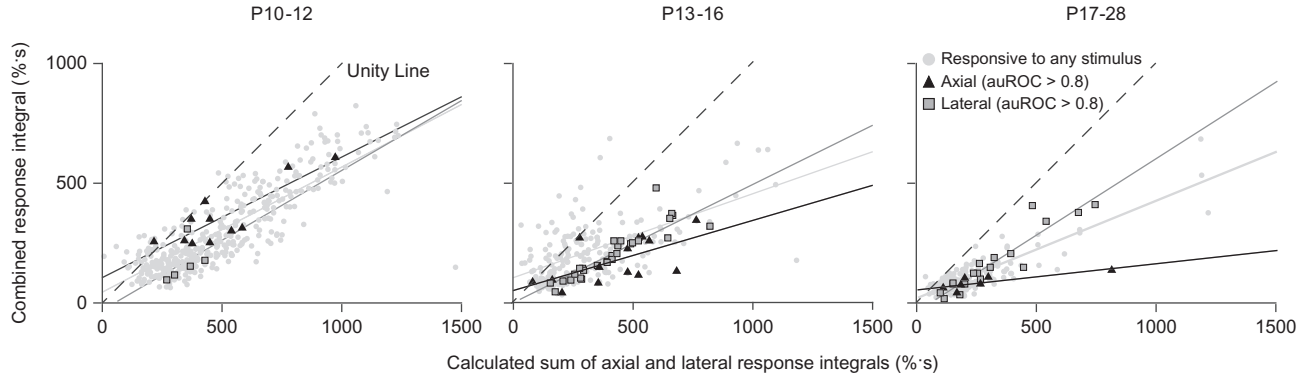

Figure 9. Sublinear responses of L2/3 neurons to combined axial-lateral whisker stimulation. Scatter distribution of responses to the combined stimulus vs. the calculated linear sum of responses to axial and lateral stimulation across age groups (left: P10–12; middle: P13–16; right: P17–28). Grey dots indicate responsive neurons, black triangles and grey squares indicate highly selective (auROC > 0.8) axial-preferring and lateral-preferring neurons, respectively. Solid lines indicate regression lines, dashed line indicates the unity line. Distributions are shown for responsive neurons of 6 animals (number of neurons: P10–12: 340; P13–16: 181; P17–28: 123). Number of highly selective neurons: Axial, P10–12: 11, P13–16: 14, P7–28: 7; Lateral, P10–12: 5, P13–16: 26, P17–28: 17.

network maturation. Our novel stimulation paradigm allowed us to study the development of selectivity for axial or lateral whisker stimuli across cortical layers in mouse barrel cortex. We found an increased proportion of stimulus-selective neurons in L2/3, L5, and L6 in animals older than P16 compared with animals younger than P13. Our imaging experiments also revealed locally intermixed populations of neurons in L2/3 selective for either axial or lateral stimuli, emerging in the critical period. These findings indicate that L2/3 is a major integration stage for processing of these whisker forces. Comparable

changes in response selectivity have also been observed in visual cortex (Rochefort et al. 2011) although sensory processing most likely undergoes different maturation processes in barrel cortex compared with visual cortex (Clemens et al. 2012; Hoy and Niell 2015). The representation of axial stimuli has previously been studied in trigeminal ganglion neurons (Stüttgen et al. 2008) but not in detail throughout a neocortical column. Studies in adult mice have shown that axial and lateral whisker-forces are important features for object localization (Pammer et al. 2013; Quist et al. 2014). The emerging response selectivity for axial or lateral forces that we found during postnatal week 3 occurs in parallel to the start of active tactile exploration. Response selectivity for axial whisker forces thus might be relevant for explorative behavior, when touch-induced forces become more complex. In line with this notion, a recent study found that neurons in L2/3 of adult mice are selectively tuned for whisker distance relative to a virtual corridor wall (Sofroniew et al. 2015). We therefore speculate that enhanced neuronal selectivity to axial/lateral force components may help the young mouse to judge object parameters such as object distance and texture during exploration. Whether changes in whisker mechanics, maturation of the whisker follicle, and changes in peripheral signal transmission may contribute to this development remains unclear, but we did not observe any obvious changes in whisker stiffness or thickness in the critical period. Future studies could investigate the maturation of peripheral and thalamocortical circuit components and their contribution to whisker-related sensory processing.

Our experimental data suggest that not only axial and lateral response selectivity increases during the critical period, especially in L2/3, but also that neuronal activity patterns evoked by these whisker force components also interact, evident in the sublinear summation of responses observed in the case of combined stimulation. The observed increase in sublinear processing with age hints towards competition of whisker-evoked inputs on the local neocortical circuit level, although on an MUA level these stimuli induce very similar response profiles. If and how this competition is facilitated by specific subsets of cells in the local circuitry of L2/3 networks, in particular inhibitory interneurons, or by modified transmission through the whisker and the follicle remains to be explored.

The maturation of cortical circuits in barrel cortex can be disrupted during early development if whiskers are plucked or trimmed (van der Loos and Woolsey 1973; Skibinska et al. 2000). Overall sparsification and decorrelation in barrel cortex is, however, believed to be intrinsically mediated in L2/3, as whisker deprivation does not alter the sparsification of spontaneous population activity (Golshani et al. 2009). It remains unclear whether emergence of response selectivity in barrel cortex is mainly driven by an intrinsic program or whether it relies on specific experience-dependent inputs during active exploratory behavior. In visual cortex, sparsification of sensory-evoked activity is delayed in dark-reared mice but selectivity emerges independent of visual input, even before eye opening (Rochefort et al., 2009; Rochefort et al., 2011). Further studies are needed to dissect intrinsic and experience-dependent mechanisms that underlie the development of response selectivity in barrel cortex. The short time window, during which most of the change happens, and the slow regrowth of whiskers will make such experiments challenging.

Our electrophysiological data also provide evidence for refined whisker-evoked adaptation and increased response selectivity in L5 and L6 after the critical period. Both EXC and INH SUs showed increased selectivity for either axial or lateral stimuli. We assume that neurons in L5, including stimulus-selective INH neurons, play an important role in processing different whisker forces for the principal whisker as L5 thick-tufted cells are major output neurons of the cortex, further conveying whisker information to downstream brain areas (de Kock et al. 2007). The exact role of specific neuronal sub-types in the developmental processes warrants further investigation.

In conclusion, we have shown that processing of sensory information in barrel cortex changes substantially within a short developmental period (between P13 and P16), in parallel to the onset of active whisking behavior. This maturation includes layer-specific changes in stimulus responsiveness and adaptation and the development of response selectivity. The development of new tools and techniques for longitudinal investigation of network maturation (e.g., expression of genetically encoded calcium indicators, or chronically implanted electrodes) might help to further dissect the underlying mechanisms and better connect the observed changes in cortical processing to behavioral adaptations.

Supplementary Material

Supplementary material can be found at: http://www.cercor.oxfordjournals.org/.

Authors' Contributions

Conceptualization, A.v.d.B, H.J.L., and F.H.; Methodology, A.v.d.B., M.W., M.C.S.; Software, A.v.d.B. and B.L.; Formal analysis, A.v.d.B., J.-W.Y., V.R.-P.; Investigation, A.v.d.B. and J.-W.Y.; Writing – Original Draft, A.v.d.B. and F.H.; Writing – Review & Editing, V.R.-P., M.C.S., H.J.L.; Visualization, A.v.d.B., J.-W. Y. and V.R.-P.; Supervision, H.J.L. and F.H.

Funding

German-Swiss Research Unit "Barrel Cortex Function" (DFG FOR1341, SNSF 310030E-147485; F.H. and H.J.L.); the Swiss National Science Foundation (SNSF, grant 31003A_149858, F.H.); the Swiss Foundation for Excellence in Biomedical Research (A.v.d.B. and F.H.); DFG (grant Lu 375/6-2, H.J.L.).

Notes

We would like to thank Fabian F. Voigt, Marco Tedaldi, Stefan Giger, Hansjörg Kasper and Beate Krumm for expert technical assistance. We would also like to thank Theofanis Karayannis, Martin Müller, Simon Musall, Philipp Bethge, and Abhishek Banerjee for valuable input on the manuscript. *Conflict of Interest*: None declared.

References

Arakawa H, Erzurumlu RS. 2015. Role of whiskers in sensorimotor development of C57BL/6 mice. Behav Brain Res. 287: 146–155.

Borgdorff AJ, Poulet JF, Petersen CCH. 2007. Facilitating sensory responses in developing mouse somatosensory barrel cortex. J Neurophysiol. 97:2992–3003.

Chandrasekaran S, Navlakha S, Audette NJ, McCreary DD, Suhan J, Bar-Joseph Z, Bartha L. 2015. Unbiased, high-throughput electron microscopy analysis of experience-dependent synaptic changes in the neocortex. J Neurosci. 35:16450–16462.

Chen JL, Carta S, Soldado-Magraner J, Schneider BL, Helmchen F. 2013. Behaviour-dependent recruitment of long-range projection neurons in somatosensory cortex. Nature. 499: 336–340.

Clack NG, O'Connor DH, Huber D, Petreanu L, Hires A, Peron S, Svoboda K, Myers EW. 2012. Automated tracking of whiskers in videos of head fixed rodents. PLoS Comp Biol. 8(7): e1002591.

Clem RL, Barth A. 2006. Pathway-specific trafficking of native AMPARs by in vivo experience. Neuron. 49:663–670.

Clem RL, Celikel T, Barth AL. 2008. Ongoing in vivo experience triggers synaptic metaplasticity in the neocortex. Science. 319:101–104.

Clemens JM, Ritter NJ, Roy A, Miller JM, Van Hooser SD. 2012. The laminar development of direction selectivity in ferret visual cortex. J Neurosci. 32:18177–18185.

de Kock CPJ, Bruno RM, Spors H, Sakmann B. 2007. Layer- and cell-type-specific suprathreshold stimulus representation in rat primary somatosensory cortex. J Physiol. 581:139–154.

Doischer D, Aurel Hosp J, Yanagawa Y, Obata K, Jonas P, Vida I, Bartos M. 2008. Postnatal differentiation of basket cells from slow to fast signaling devices. J Neurosci. 28:12956–12968.

Ebara S, Kumamoto K, Matsuura T, Mazurkiewicz JE, Rice FL. 2002. Similarities and differences in the innervation of mystacial vibrissal follicle-sinus complexes in the rat and cat: A confocal microscopic study. J Comp Neurol. 449:103–119.

Einevoll GT, Franke F, Hagen E, Pouzat C, Harris KD. 2012. Towards reliable spike-train recordings from thousands of neurons with multielectrodes. Curr Opin Neurobiol. 22:11–17.

Erzurumlu RS, Gaspar P. 2012. Development and critical period plasticity of the barrel cortex. Eur J Neurosci. 35: 1540–1553.

Feldmeyer D, Brecht M, Helmchen F, Petersen CCH, Poulet JF, Staiger JF, Luhmann HJ, Schwarz C. 2013. Barrel cortex function. Prog Neurobiol. 103:3–27.

Golshani P, Gonçalves JT, Khoshkhoo S, Mostany R, Smirnakis S, Portera-Cailliau C. 2009. Internally mediated developmental desynchronization of neocortical network activity. J Neurosci. 29:10890–10899.

Gopal V, Hartmann MJZ. 2007. Using hardware models to quantify sensory data acquisition across the rat vibrissal array. Bioinspir Biomim. 2:S135–S145.

Grant R a, Mitchinson B, Prescott TJ. 2012. The development of whisker control in rats in relation to locomotion. Dev Psychobiol. 54:151–168.

Gray CM, Maldonado PE, Wilson M, McNaughton B. 1995. Tetrodes markedly improve the reliability and yield of multiple single-unit isolation from multi-unit recordings in cat striate cortex. J Neurosci Methods. 63:43–54.

Guo ZV, Li N, Huber D, Ophir E, Gutnisky D, Ting JT, Feng G, Svoboda K. 2014. Flow of cortical activity underlying a tactile decision in mice. Neuron. 81:179–194.

Hagihara KM, Murakami T, Yoshida T, Tagawa Y, Ohki K. 2015. Neuronal activity is not required for the initial formation and maturation of visual selectivity. Nat Neurosci. 18:1780–1788.

Harris KD, Henze DA, Csicsvari J, Hirase H, Buzsaki G. 2000. Accuracy of tetrode spike separation as determined by simultaneous intracellular and extracellular measurements. J Neurophysiol. 84:401–414.

Hazan L, Zugaro M, Buzsáki G. 2006. Klusters, NeuroScope, NDManager: a free software suite for neurophysiological data processing and visualization. J Neurosci Methods. 155: 207–216.

Hoy JL, Niell CM. 2015. Layer-specific refinement of visual cortex function after eye opening in the awake mouse. J Neurosci. 35:3370–3383.

Ikezoe K, Tamura H, Kimura F, Fujita I. 2012. Decorrelation of sensory-evoked neuronal responses in rat barrel cortex during postnatal development. Neurosci Res. 73:312–320.

Itami C, Kimura F. 2012. Developmental switch in spike timing-dependent plasticity at layers 4-2/3 in the rodent barrel cortex. J Neurosci. 32:15000–15011.

Katz Y, Heiss JE, Lampl I. 2006. Cross-whisker adaptation of neurons in the rat barrel cortex. J Neurosci. 26:13363–13372.

Khazipov R, Luhmann HJ. 2006. Early patterns of electrical activity in the developing cerebral cortex of humans and rodents. Trends Neurosci. 29:414–418.

Kremer Y, Léger J-F, Goodman D, Brette R, Bourdieu L. 2011. Late emergence of the vibrissa direction selectivity map in the rat barrel cortex. J Neurosci. 31:10689–10700.

Krupa DJ, Matell MS, Brisben, AJ, Oliveira LM, Nicolelis MA. 2001. Behavioral properties of the trigeminal somatosensory system in rats performing whisker-dependent tactile discriminations. J Neurosci. 21:5752–5763.

Landers M, Philip Zeigler H. 2006. Development of rodent whisking: trigeminal input and central pattern generation. Somatosens Mot Res. 23:1–10.

Langer D, van't Hoff M, Keller AJ, Nagaraja C, Pfäffli OA, Göldi M, Kasper H, Helmchen F. 2013. HelioScan: a software framework for controlling in vivo microscopy setups with high hardware flexibility, functional diversity and extendibility. J Neurosci Methods. 215:38–52.

Lendvai B, Stern EA, Chen B, Svoboda K. 2000. Experience-dependent plasticity of dendritic spines in the developing rat barrel cortex in vivo. Nature. 404:876–881.

Maravall M, Stern EA, Svoboda K. 2004. Development of intrinsic properties and excitability of layer 2/3 pyramidal neurons during a critical period for sensory maps in rat barrel cortex. J Neurophysiol. 92:144–156.

Micheva KD, Beaulieu C. 1996. Quantitative aspects of synaptogenesis in the rat barrel field cortex with special reference to GABA circuitry. J Comp Neurol. 373:340–354.

Mitzdorf U. 1985. Current source-density method and application in cat cerebral cortex: investigation of evoked potentials and EEG phenomena. Physiol Rev. 65:37–100.

Nicholson C, Freeman JA. 1975. Theory of current source-density analysis and determination of conductivity tensor for anuran cerebellum. J Neurophysiol. 38:356–368.

Nimmerjahn A, Kirchhoff F, Kerr JND, Helmchen F. 2004. Sulforhodamine 101 as a specific marker of astroglia in the neocortex in vivo. Nat Methods. 1:31–37.

Pammer L, O'Connor DH, Hires SA, Clack NG, Huber D, Myers EW, Svoboda K. 2013. The mechanical variables underlying object localization along the axis of the whisker. J Neurosci. 33:6726–6741.

Quairiaux C, Megevand P, Kiss JZ, Michel CM. 2011. Functional development of large-scale sensorimotor cortical networks in the brain. J Neurosci. 31:9574–9584.

Quist BW, Seghete V, Huet LA, Murphey TD, Hartmann MJZ. 2014. Modeling forces and moments at the base of a rat vibrissa during noncontact whisking and whisking against an object. J Neurosci. 34:9828–9844.

Reyes-Puerta V, Sun J-J, Kim S, Kilb W, Luhmann HJ. 2015. Laminar and columnar structure of sensory-evoked multineuronal spike sequences in adult rat barrel cortex in vivo. Cereb Cortex. 25:2001–2021.

Rochefort N, Garaschuk O, Milos R, Narushima M, Marandi N, Pichler B, Kovalchuk Y, Konnerth A. 2009. Sparsification of neuronal activity in the visual cortex at eye-opening. Proc Natl Acad Sci USA. 106:1–6.

Rochefort NL, Narushima M, Grienberger C, Marandi N, Hill DN, Konnerth A. 2011. Development of direction selectivity in mouse cortical neurons. Neuron. 71:425–432.

Sakata S, Harris KD. 2009. Laminar structure of spontaneous and sensory-evoked population activity in auditory cortex. Neuron. 64:404–418.

Simons DJ. 1983. Multi-whisker stimulation and its effects on vibrissa units in rat SmI barrel cortex. Brain Res. 276:178–182.

Skibinska A, Glazewski S, Fox K, Kossut M. 2000. Age-dependent response of the mouse barrel cortex to sensory deprivation: a 2-deoxyglucose study. Exp Brain Res. 132:134–138.

Sofroniew NJ, Vlasov YA, Andrew Hires S, Freeman J, Svoboda K. 2015. Neural coding in barrel cortex during whisker-guided locomotion. eLife. 4:1–36.

Stern EA, Maravall M, Svoboda K. 2001. Rapid development and plasticity of layer 2/3 maps in rat barrel cortex in vivo. Neuron. 31:305–315.

Stosiek C, Garaschuk O, Holthoff K, Konnerth A. 2003. In vivo two-photon calcium imaging of neuronal networks. Proc Natl Acad Sci USA. 100:7319–7324.

Stüttgen MC, Kullmann S, Schwarz C. 2008. Responses of rat trigeminal ganglion neurons to longitudinal whisker stimulation. J Neurophysiol. 100:1879–1884.

Thévenaz P, Ruttimann UE, Unser M. 1998. A pyramid approach to subpixel registration based on intensity. IEEE Trans Image Process. 7:27–41.

van der Loos H, Woolsey TA. 1973. Somatosensory cortex: structural alterations following early injury to sense organs. Science. 179:395–398.

Wen JA, Barth AL. 2011. Input-specific critical periods for experience-dependent plasticity in layer 2/3 pyramidal neurons. J Neurosci. 31:4456–4465.

Woolsey TA, van der Loos H. 1970. About the physiological organization of the cerebral cortex of the mouse and the rat in which the shape, size, organization and number of the barrels is particularly. Brain Res. 17:205–242.

Yang JW, Hanganu-Opatz IL, Sun JJ, Luhmann HJ. 2009. Three patterns of oscillatory activity differentially synchronize developing neocortical networks in vivo. J Neurosci. 29: 9011–9025.

Yu X, Chung S, Chen D-Y, Wang S, Dodd SJ, Walters JR, Isaac JTR, Koretsky AP. 2012. Thalamocortical inputs show post-critical-period plasticity. Neuron. 74:731–742.

Zhang Z, Jiao YY, Sun QQ. 2011. Developmental maturation of excitation and inhibition balance in principal neurons across four layers of somatosensory cortex. Neuroscience. 174:10–25.